

# Functional Manufacturing and Mechanical Dynamics II

Edited by  
Hun Guo, Taiyong Wang, Zeyu Weng, Weidong Jin,  
Shaoze Yan, Xuda Qin, Guofeng Wang,  
Qingjian Liu and Zijing Wang

# **Functional Manufacturing and Mechanical Dynamics II**

Edited by  
Hun Guo  
Taiyong Wang  
Zeyu Weng  
Weidong Jin  
Shaoze Yan  
Xuda Qin  
Guofeng Wang  
Qingjian Liu  
Zijing Wang

# **Functional Manufacturing and Mechanical Dynamics II**

Selected, peer reviewed papers from the  
2012 International Conference on  
Functional Manufacturing and Mechanical Dynamics,  
January 22-25, 2012, Hangzhou, Zhejiang, China

*Edited by*

**Hun Guo, Taiyong Wang, Zeyu Weng, Weidong Jin,  
Shaoze Yan, Xuda Qin, Guofeng Wang,  
Qingjian Liu and Zijing Wang**



**Copyright** © 2012 Trans Tech Publications Ltd, Switzerland

All rights reserved. No part of the contents of this publication may be reproduced or transmitted in any form or by any means without the written permission of the publisher.

Trans Tech Publications Ltd  
Kreuzstrasse 10  
CH-8635 Durnten-Zurich  
Switzerland  
<http://www.ttp.net>

Volume 141 of  
*Applied Mechanics and Materials*  
ISSN 1662-7490

Full text available online at <http://www.scientific.net>

***Distributed worldwide by***

Trans Tech Publications Ltd  
Kreuzstrasse 10  
CH-8635 Durnten-Zurich  
Switzerland

Fax: +41 (44) 922 10 33  
e-mail: [sales@ttp.net](mailto:sales@ttp.net)

***and in the Americas by***

Trans Tech Publications Inc.  
PO Box 699, May Street  
Enfield, NH 03748  
USA

Phone: +1 (603) 632-7377  
Fax: +1 (603) 632-5611  
e-mail: [sales-usa@ttp.net](mailto:sales-usa@ttp.net)

## Preface

In order to improve the development of the academy and its international influence, some excellent papers were selected to publish in the international periodical. All the papers submitted were refereed by the academic committee of Functional Manufacturing and Mechanical Dynamics I, and well-known professors and experts. Based on the referees' comments, about 114 papers are finally selected for the conference presentation and inclusion in the proceedings, and all the papers are edited by the secretariat of academic committee.

As Chairman of Functional Manufacturing and Mechanical Dynamics, I would like to take this opportunity to express my appreciation of the kind support and high quality contributions by all contributors and delegates. Equally, my thanks are extended to all conference organizers, supporters, and co-sponsors for their generous contribution. Thanks are also given to Associate prof. Hun Guo, Associate prof. Weidong Jin, Dr. Qingjian Liu for their editing work, and to Trans Tech publications for publishing the volume.

*Professor Taiyong Wang*

*Chairman, the 2<sup>nd</sup> International Conference of Functional Manufacturing and Mechanical Dynamics*

Conference organizers

Tianjin University

Zhejiang University of Technology

# Table of Contents

## Preface

## Chapter 1: Vibration Technology

<b>A Built-in Force Actuator for Active Unbalanced Vibration Control of Grinding Wheel</b> X.L. Qiao and C.S. Zhu	3
<b>A Theoretical Model for Calculating Vibration Characteristics of A Kind of Driver Seat with Air Spring and MR Damper</b> X.X. Zhu and S.H. Zhu	8
<b>Aeroengine Oil Fault Diagnosis Based on D-S Evidential Theory</b> H.C. Qu, X.B. Ding and T.Y. Wang	15
<b>Application of Generalized Stochastic Resonance to the Vibration Test</b> Y. Zhang and S.M. Li	21
<b>Conceptual Design of Hybrid-Driven Precision Press</b> Y.G. Li and B. Yan	26
<b>Control Strategy for Multi-Exciter Random Vibration Test</b> D.J. Chen, J.Y. Chen, X.Q. Shen and Z.W. Chen	33
<b>Design Strategy of Tightening Spindle System on the Principle of Modularity</b> Y.W. Zhang and J.G. Yang	39
<b>Experimental and Numerical Analysis for Two Kinds of Impact Vibration of Gear</b> L.Y. Su, Y.Q. Sun and J.M. Wen	43
<b>Low-Frequency Shaking of the Construction Machine Cab and Design of Vibration Isolators for Protecting</b> X.J. Sun and J.R. Zhang	49
<b>One-Dimensional Bi-Stage Phononic Band Gap Shaft Structure for Reducing Torsional Vibration</b> L.X. Li, T.N. Chen, X.P. Wang and B. Li	54
<b>Principle and Application of Free Resonance Vibration Isolation Based on Dry Friction Damper</b> H.J. Yu and X.L. Yan	59
<b>Study on Vibration Modes and Acoustic Radiation Modes for Air Conditioning Compressor</b> M. Yu, L.L. Zhang, Y. Li, X.G. Yan and J. Du	64

## Chapter 2: Mechanical Dynamics

<b>An Experiment Study on the Dynamic Characteristics of Linear Rolling Guide</b> L.B. Zhao, Z.Y. Weng, H.G. Ding, X.Q. Shen and X.Z. Tang	71
<b>Analysis and Calculation of Vacuum Film Deaeration for High Viscosity Liquids</b> X.B. Liu, J.R. Zhang, P. Li and X.H. Wang	76
<b>Application Research for Super-Gaussian Random Vibration Test Control Strategy</b> Z.W. Chen, X. Wen and D.J. Chen	83
<b>Application Research of Improved BP Algorithm</b> C. Yang and C. Shi	88
<b>Based on GA Mixed with Trust Region Method Solving Nonlinear Least Square Problems</b> M. Hu, T.Y. Wang, B. Geng, Q.C. Wang and D.P. Li	92
<b>Deployment Simulation of Mooring Buoy System</b> Z.Y. Chang, L. Wang, D.X. Gao and Z.Q. Zheng	98
<b>Design of Distributed Wireless Monitoring System to Photovoltaic Modules Based on CC2530</b> B.J. Xu and M. Wang	103
<b>Dynamic Analysis of Giant Magnetostrictive Actuator with Temperature and <math>\Delta E</math> Effect Accounted</b> H.Q. Yuan, W.B. Wu, D. Li and Y. Li	109

<b>Dynamic Mechanism Research and Seismic Simulation Experimentation on Superconducting Busbar of the ITER</b> K.S. Wang and Y.T. Song	114
<b>Dynamic Modeling of CNC High Precision Surface Grinding Machine with Horizontal Spindle and Rotary Table MGK7350</b> X.X. Lin, Z.Y. Weng, B. Lu, T. Yang and H.G. Ding	119
<b>Dynamic Performance Extraction and Recognition of the PT Speed Governor Based on Mathematical Morphology</b> X.Q. Wang, D. Wang, S. Liang and H.J. Zhu	124
<b>Dynamics Characteristic Analysis of Deliberate Mistuned Bladed-Disk System in Compressor Based on Substructure Method</b> H.Q. Yuan, L. Zhang and L. Song	129
<b>The Finite Element Analysis of Vibrating Screen</b> C.G. Ding, F.Z. Song, B. Song and X.H. Men	134

### Chapter 3: Functional Manufacturing and Information Technology

<b>A Euclidean Distance Optimization Model of Manufacturing Task Parameters for Collaborative Manufacturing Chain of Virtual Enterprises</b> F.Q. Cheng	141
<b>A Mathematical Model for Frost Formation on Ground Aircraft</b> L.W. Wang, D.D. Xu and Z.W. Xing	147
<b>A New Interpolation Algorithm for Auto Machining Technology of 3-D Profile of Die Edge</b> T. Wang, Y.J. Cai and G.H. Li	152
<b>A Nonlinear PID Controller for Electro-Hydraulic Servo System Based on PSO Algorithm</b> J.P. Chen, B.C. Lu, F. Fan, S.C. Zhu and J.X. Wu	157
<b>A Stochastic-Based Method for Finite Element Model Validation</b> S.F. Bi and Z.M. Deng	162
<b>Abnormal Noise Diagnosis of Internal Combustion Engine Using Wavelet Spatial Correlation Filter and Symmetrized Dot Pattern</b> C. Yang and T. Feng	168
<b>Adaptive Quadrant Error Compensation of Embedded CNC System Based on ARM and DSP</b> Y.Y. Ding, G.F. Wang, Z.F. Qiao, Z.Y. Tang and X.G. Ling	174
<b>Aeroelastic Analysis of Supersonic Airfoil with Hysteretic Nonlinearities</b> M.X. Fang	180
<b>An Algorithm for Space Tool Compensation Used in Five-Axis Numerical Control System</b> L. Zhao, J.C. Dong, Z.F. Qiao, Y.Y. Ding and Z.Y. Tang	186
<b>An Effective Method for Determining Finite Element Model Parameters of Rotor Elastic Support System</b> Y.X. Wang, J. Yan and S.Z. Wang	191
<b>An Interface Design of Communication between PC104 and DSP Based on Dual-Port RAM</b> B. Li, Q.J. Liu, Z.F. Qiao, J.C. Dong and Q. Liu	198
<b>Analysis and Simulation of Screw Joint in CNC Machine Tool</b> Y.W. Zhang and W.M. Zhang	203
<b>Analysis of Dynamics Characters of Bed Structure of CNC Machine Tool on FEM Method</b> Y.W. Zhang and W.M. Zhang	208
<b>Analysis of Natural Frequency of Simply Supported Beam with Vertical Elastic Constraint</b> B. Geng, M. Hu, Q.C. Wang, J.Z. Lin and D.P. Li	212
<b>Bearing Elevation Monitoring Instrument and its Application on Multi-Support Turbo-Generator Unit</b> Y.J. Guo, Y.W. Tian, J.Y. Liu, Y.W. Bai and W.T. Zhang	218
<b>Behaviour of Tube under Axial Crush Load with Considering Effect of Heat Exchanged</b> X.S. Dai and J.M. Ma	224
<b>Design and Implementation of Modular FPGA-Based Multiple-Axis Motion Controller for CNC</b> X.G. Ling, Q. Li, Y.Y. Ding, Z.Y. Tang, Y.Y. Ding and J.B. Xun	233

<b>Design of Automatic Assembly System of Saw Chain</b> Z.X. Ding, F. Yuan and J. Zhu	239
<b>Development of a Master-Slave Architecture Handheld Rotating Machine Fault Diagnosis Instrument</b> J. Wan, T.Y. Wang, J.C. Dong, P. Zhang and Y. Hao	244
<b>Development of an Ontology-Based and STEP-Compliant Intelligent CNC System</b> P. Li, T.L. Hu and C.R. Zhang	251
<b>Digitally Reverse Modeling for the Repair of Blades in Aero-Engines</b> T. Wang, Y.L. Liu, L.W. Wang, H. Wang and J. Tang	258
<b>Error Analysis and Calibration of Gyro-Stabilized Platform for Electro-Optical Pointing System</b> X.Y. Zhou, Y.F. Lu, Z.Y. Zhang and D.P. Fan	264
<b>Evaluation and Design of SNS User Interface in Handheld Device Based on Fuzzy Clustering</b> R. Tian, Q.S. Xie and L.W. Shi	270
<b>Experimental Research on the Crack Identification of Drawing Parts Based on AE Technique</b> Z.G. Luo, B.G. Zhang and X. He	275
<b>Extraction of Frequency-Variable Characteristics and Analysis of Modulation Mechanism under Periodic Excitation</b> X.Q. Wang, Y. Zhao, S. Liang and S.H. Qian	279
<b>Failure Mode, Effect and Criticality Analysis of CNC Grinder</b> H.J. Wang, L. Sun and L. Shi	284
<b>Finite Element Analysis of the Helical Surface Cutting Tool</b> X.W. Sun, H. Wang, K. Wang and X. Feng	289
<b>Finite Element Simulation of Extremely High Speed Machining of Ti6Al4V Alloy</b> Y. Tan, Y.L. Chi, Y.Y. Huang and T.Q. Yao	293
<b>Four-Point Regulation Algorithm for an End-Effector of a Flexible Drilling Robot</b> L.X. Zhang and X.S. Wang	298
<b>Fuzzy Sliding Mode Control for a Three-Links Spatial Robot Based on RBF Neural Network</b> S.B. Hu and M.X. Lu	303
<b>Helmholtz Resonator with Extended Neck and Absorbing Material</b> R. Bi, Z.S. Liu, K.M. Li, J. Chen and Y. Wang	308
<b>Influence of Crank Radius on the Curve Shapes for a Multi-Link High-Speed Precision Press</b> X.J. Lu, S.H. Zhu, Z.M. Ke, J. Qin and S. Wei	313
<b>Influence of Vehicle Suspension System on Ride Comfort</b> J.Z. Xia, Z.P. Ma, S.M. Li and X.B. An	319
<b>Interior Acoustic Field Analysis of Hydraulic Excavator's Cabin Based on Bem</b> Y. Wang, J.R. Zhang, X.B. Liu and V. Le	323
<b>Investigation of Laser Parameters Influence of Direct-Part Marking Data Matrix Symbols on Aluminum Alloy</b> H.D. Qiu, W.S. Bao and C.H. Lu	328
<b>Kinematics and Kinetostatic Analysis of a New Type of Mechanical Excavator with Controllable Mechanism</b> Y.C. Pan, G.W. Cai, Z. Zhang, Y. Chen and Y.Z. Li	334
<b>Machining Theory of Forming Complex Inner Helicoid and Numerical Algorithm to Design Contour of the Disc-Mill Cutter</b> K. Wang, S.Q. Wang, X.W. Sun and G.D. Liu	339
<b>Measurement and Analysis of Cutting Force and Optimization of Cutting Parameters by High Speed Milling</b> H.Z. Li, Y. Wang, N.X. Zhu, R.B. Hu, C. Zhang and F.B. Wang	344
<b>Modeling and Identification for Lightweight High-Speed Machines with Loads Variation</b> S.X. Fan, D.P. Fan and R. Nagamune	350
<b>Modeling and Simulation of Aircraft on Ground Deicing Process Based on Thermal Balance</b> B. Chen and L.W. Wang	355
<b>Modeling and Simulation of Clamp Band Dynamic Envelope in a LV/SC Separation System</b> J.L. Li, S.Z. Yan and X.F. Tan	359

<b>Modeling and Simulation of Full-Float Tractor Cab Suspension System Based on ADAMS</b> L. He, S.H. Zhu and H.L. Zhu	364
<b>Module Partition and Evaluation Method of NC Spiral Bevel Gear Machine Tools</b> Z.G. Han and M. Hu	370
<b>NC Machining Simulation of Spiral Bevel Gear Based on VERICUT</b> Y. Wang, J.C. Dong, T.Y. Wang and L. Zhao	376
<b>Numerical Prediction on Noise from Axial Flow Fan Based on Modified Blade Force Model</b> C.J. Wu and X.Y. Zhang	381
<b>Numerical Study on Structural Improvement of the Grill Fixed at the Outlet of the Air Conditioner Outdoor Unit</b> Y. Liu and C.J. Wu	386
<b>NURBS Curve Design and CNC Machining Principle</b> B.Y. Peng and Q.S. Han	392
<b>Online Identification of the Bearing Dynamic Parameters for Rotor-Bearing Systems</b> C.L. Liu, S.P. Zhou, Y. Di and P.R. Xie	397
<b>Optimization of Milling Parameters Based on Genetic Algorithm</b> Q. Li, R. Wang, Q.J. Liu, R.Z. Wu, M.K. Shao and C.J. Liao	403
<b>Pneumatic Mechanism of Gas Cooled or Heated Through a Throttle Orifice</b> Y.B. Yin and L. Li	408
<b>Precision Analysis for Large-Travel Rotational Butterfly Pivot</b> Y.F. Lu, X.Y. Zhou, D.P. Fan and Z.Y. Zhang	413
<b>Processing Parameters Optimization Based on PSO Algorithm</b> R.Z. Wu, Q.J. Liu, M.K. Shao and R. Wang	419
<b>Research of the Soft PLC Based on the Open PLC</b> Z.Y. Tang, J.C. Dong, Z.F. Qiao, X.G. Ling, Y.Y. Ding and J.B. Xun	424
<b>Research on Integrated Architecture for Tool Wear Monitoring System of CNC Machine Center</b> Q. Ning, Q.J. Liu and L. Liu	429
<b>Research on Mechanical Fault Diagnosis Based on Cascaded Bistable Stochastic Resonance and Fractal Box Dimension</b> Y. Hao, J.C. Dong, T.Y. Wang, J. Wan and P. Zhang	434
<b>Research on Post Processing of 5-Axis Linkage Machines</b> M.K. Shao, Z. Wang, J.Z. Zhi, R.Z. Wu and R. Wang	438
<b>Research on Power Flow Transmitted through Rolling Bearing in the Gear Shaft-Plate Coupled Structure</b> X.F. Zhang, R. Huo, Y.Q. Zhou and Z. Zhou	442
<b>Research on Subdivision Interpolation for High Speed CNC Applications</b> J.C. Dong, Q.J. Liu and T.Y. Wang	449
<b>Research on the Information Extraction Technology of STEP</b> X.B. Liu, W. Zhao, C.N. Li and D.J. Hu	455
<b>Research on the Post-Processing Algorithm about Five-Axis High-Speed Machine Center</b> W. Zhao, T.A. Hadush and Q.Y. He	460
<b>Research on the Remote Monitoring and Fault Diagnosis of CNC System Based on Network</b> J.Z. Lin, D.Y. Jiang, B. Geng and Z.H. Zhang	465
<b>Research on the Vibration of Sheet Metal near the Zinc Pot Area in Continuous Hot-Dip Galvanizing Line</b> P.M. Xu, B. Wang, J.J. Ye, H.J. Zhang, Z.L. Huang and X.K. Xu	471
<b>Resin Concrete Specimens Attenuation Characteristics Research</b> H.G. Ding, Z.Y. Weng, H.W. You, B. Lu and X.Z. Tang	478
<b>Signal Feature Extraction about the Oil Whirl and Oil Oscillation Based on EMD</b> B.J. Xu and R. Liu	483
<b>Singularity Analysis of Limited-DOF Parallel Manipulator Based on Jacobian Matrixes</b> X.Y. Li and W.Y. Chen	488
<b>Smart Reverse Supply Chain: An Application of IoT to Green Manufacturing</b> X.Q. Xu, C. Jin and Y.D. Cao	493
<b>Software Development of Portable Data-Acquisition and Signal Analysis Instrument Based-on Qt</b> D.Y. Jiang and J.Z. Lin	498

<b>SR Recovery Methodology Based on the Signal Classification</b> P. Zhang, J.C. Dong, T.Y. Wang, J. Wan and Y. Hao	503
<b>Stability Analysis of Turning Process Based on a 2-DOFs Model with Overlap Factor</b> L.X. Zhang, X.S. Wang and S.L. Liu	508
<b>Strength Optimization Design of Box-Shape Arms of a Scissor Lift Mechanism with Single Hydraulic Cylinder</b> W. Zhang, X.X. Wang and L.W. Wang	513
<b>Study of Camshaft Grinders Faults Prediction Based on RBF Neural Network</b> T. Dong, H.J. Wang and L. Shi	519
<b>Study on Post-Processing of Five-Axis Cnc Machining</b> J.Z. Zhi, C.Z. Ren and J.C. Dong	524
<b>Study on the Test Method for High Temperature and Heavy Loaded Grease Bearing Life</b> Y.G. Xu, Z.Y. Weng, H.W. You, Y.Q. Zheng and X.P. Huang	529
<b>The Analysis of Transient Stability for Four Wheel Steering Automobile with Proportional Control</b> Z.J. Song	534
<b>The Comparison of Acoustic Emission with Vibration for Fault Diagnosis of the Bearing</b> X.L. Feng, G.F. Wang, X.D. Qin and C. Liu	539
<b>The Design of Modal Analysis System Based on an Improved Algorithm of Discrete Orthogonal Polynomial</b> Z.W. Chen, L. Yuan and Y.C. Hu	544
<b>The Development of DNC Transfer Software Used in CNC Machine Tools</b> J.B. Xun, G. Wang, Z.F. Qiao, Y.Y. Ding, X.G. Ling and Z.Y. Tang	550
<b>The Effect of the Restrictor Structural Parameters on the Static Properties of the Aerostatic Guide Way by Finite Element Analysis</b> H.P. Li, P. Ma and B. Zhou	554
<b>The Machining Parameters Online Monitoring Method for Stability Prediction</b> Y.X. Jiang, S.P. Deng, Y.M. Qi and B. Du	559
<b>The Online Monitoring of Surface Quality Based on Time-Frequency Spectrum Analysis of Acoustic Emission</b> C. Liu, G.F. Wang, X.D. Qin and L. Zhang	564
<b>The Optimization Design and Analysis of Motorcycle Frame Structure</b> J. Wang, J. Zhou, B.B. Li, X.L. Li and S.Y. Song	569
<b>Tool Wear Monitoring in Milling Processes Based on Time-Frequency Analysis of Acoustic Emission</b> L. Zhang, G.F. Wang, X.D. Qin and X.L. Feng	574
<b>Vehicle Frame Fatigue Life Prediction Based on Finite Element and Multi-Body Dynamic</b> S.H. Zhu, Z.J. Xiao and X.Y. Li	578

## Chapter 4: Other

<b>Application of Growth Production Design DNA Calculation Inference on the Building Process of Packing Product Line Virtual Prototype</b> L.W. Shi, Q.S. Xie and R. Tian	589
<b>Reliability Analysis Based on Efficient Simulation</b> X.S. Gong and G.Q. Zhang	594
<b>Research on Ride Comfort of Off-Road Vehicles</b> J.Z. Xia, Z.P. Ma, S.M. Li and X.B. An	601
<b>Study on an EV Traction Control Strategy</b> S.R. Yan and S.Z. Li	605
<b>Technology of Magnetic Flux Leakage Signal Detection Based on Scale Transformation Stochastic Resonance</b> Y.S. Peng, Y.G. Leng and J. Wan	611
<b>Test Methods for Durability of Electric Nail Gun</b> H.G. Ding, Y.Q. Zheng, L.J. Song and Z.Y. Weng	616

**CHAPTER 1:**  
**Vibration Technology**

## **A Built-In Force Actuator for Active Unbalanced Vibration Control of Grinding Wheel**

Qiao Xiaoli<sup>1, 2, a</sup>, Zhu Changsheng<sup>1, b</sup>

<sup>1</sup>College of Electrical Engineering, Zhejiang University, Hangzhou, Zhejiang, China

<sup>2</sup>Departments of Mechatronic Engineering, Shaoxing College of Arts and Sciences, Shaoxing, Zhejiang, China

<sup>a</sup>qiaoxiaoli168@163.com, <sup>b</sup>cszhu@hotmail.com

**Key words:** Grinding wheel unbalanced vibration; Vibration control; Force actuator

**Abstract.** To effectively control unbalanced vibration caused by grinding wheel mass unbalance, a new active control strategy for grinding wheel unbalanced vibration is proposed in the paper, the controllable electromagnetic force which is used to suppress vibration in control scheme originates from the principle of a bearingless motor having a radial magnetic force generation. First, induction electric spindle radial control force model and the force model which is exerted on grinding wheel are analyzed. And then, the dynamic model of induction-type flexural electric spindle-grinding wheel is modeled using finite element method. Finally, an active unbalanced vibration control system for electric spindle-grinding wheel is designed and simulated. The results show that the control scheme has significant effect on suppressing the unbalanced vibration of grinding wheel.

### **Introduction**

High-speed grinding technology is a revolutionary jump in grinding process, its advantages mainly include grinding efficiency can be increased, machining accuracy can be improved, grinding ration of grinding wheel can be significantly increased and grinding process is easy to be automated. However, the surface quality of the workpiece and the durability of the grinding wheel would be decreased caused directly by the grinding wheel vibration, and further more, the wheel vibration may decrease the efficiency of the grinding, exacerbate the damage of grinder parts, and even cause noise to deteriorate the working conditions. So in recent years, more and more attention has been paid on the study on Dynamic Unbalanced Technology of the grinding wheel and the spindle system, especially on the dynamic characteristics of spindle - wheel system [1].

There are many dynamic balancing devices for suppressing unbalanced vibration of grinding wheel at home and abroad, the balancing devices include: balancer, damping balancer, the external actuator [2, 3] and so on. Although the balancing effects of these devices are not bad under certain conditions, these devices are external, they are bound to change the structure of spindle-grinding wheel system. In addition, these devices are not only bulky and difficult to be controlled, but also the rigid spindle could be turned into flexible spindle in high speed, the changes in balancing conditions may lead to the failure for unbalanced vibration control. To compensate for these deficiencies, an active unbalanced vibration control scheme with built-in force actuator for grinding wheel based on double windings induction bearingless motor is proposed, the scheme is used to actively control grinding wheel unbalanced vibration by means of a controllable, non-contact electromagnetic force caused by a set of control windings which are added to induction motor stator windings to form double-windings structure. The built-in force actuator does not need extra space, and will not affect the machining efficiency. The biggest advantage of the method is that it needs no other additional balance equipment.

### Radial Vibration Control Force Model

Due to asymmetric air-gap magnetic field in double-windings motor, the surface tension of rotor is no longer zero in the radial, the controllable radial force can be controlled by changing current in control windings. The control force model of spindle in  $x, y$  direction can be described as [4]:

$$\begin{bmatrix} F_{c,x} \\ F_{c,y} \end{bmatrix} = K_1 \begin{bmatrix} \Psi_{4mx} & \Psi_{4my} \\ \Psi_{4my} & -\Psi_{4mx} \end{bmatrix} \begin{bmatrix} i_{2x} \\ i_{2y} \end{bmatrix} \quad (1)$$

where  $K_1 = 9\mu_0 l r N_4 N_2 / (8\pi\delta_0^2 L_{4m})$ ,  $N_4$  and  $N_2$  is effective turns per phase of torque windings and control windings in series respectively,  $\mu_0$  the free space permeability,  $l$  the length of motor core,  $r$  rotor diameter,  $L_{4m}$  the mutual inductance between torque windings and rotor windings,  $\Psi_m$  torque winding air-gap flux.

### High-speed Grinding Wheel Model

The radial force between grinding wheel and workpiece is defined as  $x$  direction, the grinding wheel with the unbalanced force and grinding force is shown in Fig 1. In Fig,  $\varepsilon$  is the mass eccentricity of the grinding wheel,  $\theta$  counterclockwise rotation of vector  $\overline{O\varepsilon}$ ,  $F_\varepsilon$  the unbalanced force which is exerted on grinding wheel,  $F_{gt}$  the tangential force component and  $F_{gn}$  the normal component.

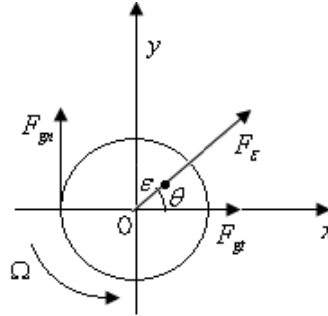


Fig. 1 Forced grinding wheel

The force exerted on wheel includes: grinding force and unbalanced force.

Grinding force originates from elastic deformation, plastic deformation and chip formation process caused by the workpiece in contact with the grinding wheel and the friction between the workpiece surface and the binder and the abrasive. If it is assumed that the effects of ploughing and sliding are not time-varying, the forces for dynamic conditions can be derived as [5]:

$$F_{gt} = u_{ch} b \delta_w v_w / v_g, \quad F_{gn} = \alpha F_{gt} \quad (2)$$

where  $u_{ch}$  is taken to be a constant and called the specific chip formation energy,  $b$  the width of the grinding wheel in cut and  $\delta$  the depth of material being removed from workpiece,  $v_w$  the surface speed of the workpiece and  $v_g$  that of the grinding wheel speed,  $\alpha$  grinding force ration, a constant relate to material properties.

The unbalanced force components in  $x, y$  direction can be formulated as:

$$F_{\varepsilon x} = M \varepsilon \Omega^2 \cos \theta, \quad F_{\varepsilon y} = M \varepsilon \Omega^2 \sin \theta \quad (3)$$

where  $M$  is grinding wheel mass,  $\Omega$  spindle speed.

### Flexible Electric Spindles –Grinding Wheel System Dynamic Model

Spindle-grinding wheel system is composed of rotor, shaft sections with distributed mass, Tool holder and grinding wheel and so on. The spindle-grinding wheel system can be divided into discs, shafts, bearings, Tool holder and grinding wheel along the axis of spindle. Each element is connected to each other in element node. These nodes are located at disc center, spindle center and some position of the spindle axis and are numbered according to the order number. In order to reduce the computation, it is simplified as follows:(1)angular contact ball bearings is simplified as rigid bearings, namely, radial stiffness is infinite. (2) the rotor, the wheel handle and the grinding wheel are assumed to be equivalent to the materials with same density.

According to the above simplification, the finite element model of spindle-grinding wheel system is established as shown in Fig 2[6]:

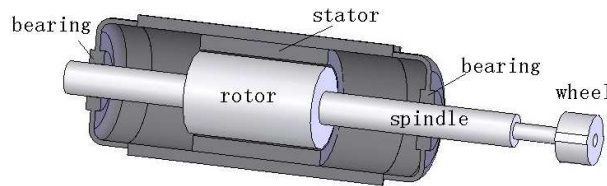


Fig. 2 Simplified finite element model of spindle-grinding wheel

After combining motion equations of every shaft section, disc, bearing, wheel handle and gringding wheel, the differential equations of spindle-grinding wheel can be obtained as:

$$M\{\ddot{U}\} + (D + \Omega G)\{\dot{U}\} + K\{U\} = \{F_e\} + \{F_g\} + \{F_c\} \quad (4)$$

where,  $U = [x_1, \theta_{y1}, \dots, x_n, \theta_{yn}, y_1, -\theta_{x1}, \dots, y_n, -\theta_{xn}]^T$ ,  $K$ ,  $D$  and  $G$  is mass matrix, inertia matrix, stiffness matrix, damping matrix and gyroscopic matrix,  $F_e$  unbalanced force,  $F_g$  grinding force,  $F_c$  control force,  $n$  is total nodes of spindle-tools system.

### Flux Identification

The radial control force model (equation (3)) shows that as long as the air-gap flux can be identified online, we can control radial force by controlling the current in control windings to suppress vibration. At stationary two phase  $x, y$  axis, the identified stator flux of torque windings based on U-I model can be derived as [7]:

$$\begin{aligned} \Psi_{4msx} &= \int (u_{4sx} - i_{4sx} R_{4s}) dt \\ \Psi_{4msy} &= \int (u_{4sy} - i_{4sy} R_{4s}) dt \end{aligned} \quad (5)$$

where  $u_{4sx}$ ,  $u_{4sy}$  and  $i_{4sx}$ ,  $i_{4sy}$  are stator voltage components and current component of torque windings at stationary 2- phase,  $R_{4s}$  is stator resistance.

According to the relationship between air-gap flux and stator flux, the air-gap flux of torque windings at the two phase stationary axis can be obtained as follows:

$$\begin{aligned} \Psi_{4mx} &= \Psi_{4msx} - L_{4s\sigma} i_{4sx} \\ \Psi_{4my} &= \Psi_{4msy} - L_{4s\sigma} i_{4sy} \end{aligned} \quad (6)$$

where  $L_{4s\sigma}$  is leakage inductance.

### Active Vibration Control System for Induction Spindle

To control unbalanced vibration of grinding wheel, the active vibration control scheme for flexible spindle-grinding wheel unbalanced vibration is designed as shown in Fig 3. The inverter is applied to control spindle speed, the identified air-gap flux online scheme is used to control wheel vibration independently. In Fig 3, the above dashed box is torque control of dual windings induction spindle, the speed errors is used as inverter input signal to control the spindle's speed.

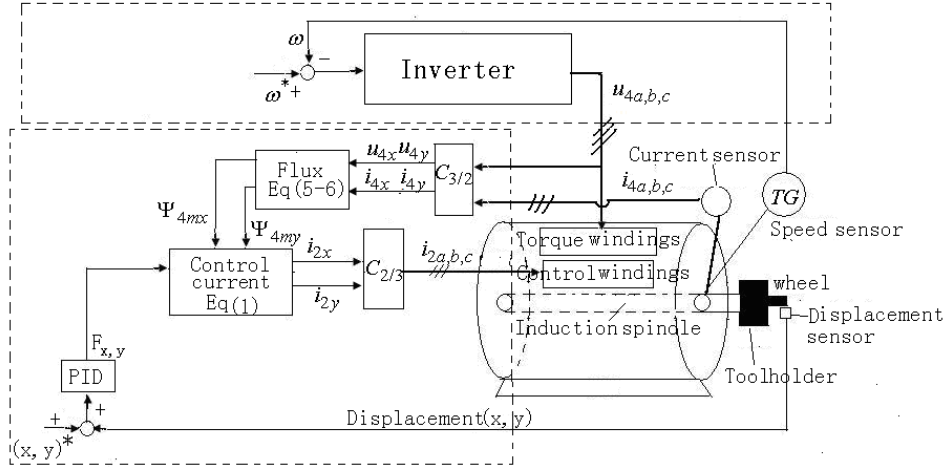


Fig. 3 Active unbalance vibration control system for induction spindle

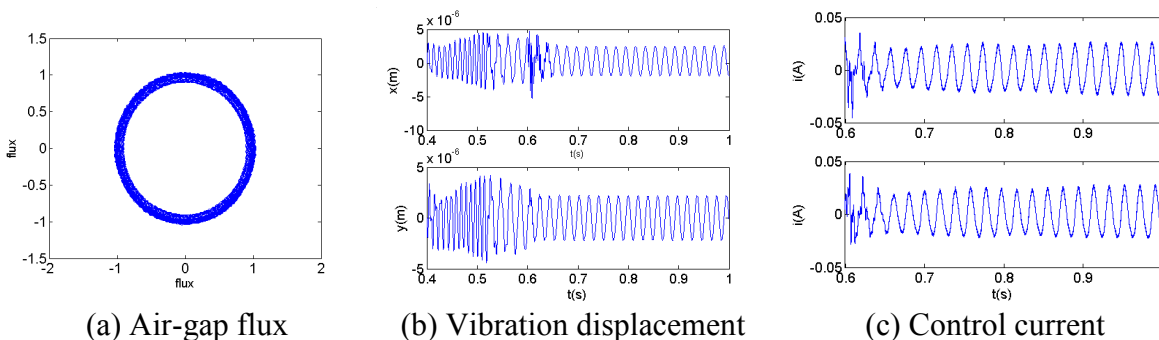
The below dashed box is unbalanced vibration control, the displacement errors at stationary  $x, y$  axis is inputted to the PD controller to generate reference force, and air-gap flux identified online at  $x, y$  axis by flux identification model are used to produce referent current at  $x, y$  axis which control windings needs, the 3- phase control current commands can be obtained from  $C_{2/3}$  transformation in order to control grinding wheel's unbalanced vibration.

### Results Analysis

This control scheme is simulated under the action of unbalance ( $100 \text{ g} \cdot \text{mm}$ ) with PD controller. The control system is simulated at  $\Omega = 6000 \text{ r/min}$  and the controller start to work at  $t = 0.6 \text{ s}$ . The air-gap flux in  $x, y$  axis, wheel's vibration displacement in  $x, y$  direction and the control effects are analyzed. Simulation parameters are given as follows:

$$P_{N1} = 38 \text{ kW}, \quad J = 1.662 \text{ kgm}^2, \quad \delta_0 = 375 \mu\text{m}, \quad p_4 = 2, \quad R_{4s} = 0.087 \Omega, \quad R_{4r} = 0.228 \Omega, \\ L_{4s} = L_{4r} = 35.5 \text{ e-}3 \text{ H}, \quad L_{4m} = 34.7 \text{ e-}3 \text{ H}, \quad p_2 = 1, \quad L_{2m} = 0.00932 \text{ H}, \quad R_{2s} = 1.03 \Omega, \quad R_{2r} = 0.075 \Omega. \\ u_{ch} = 1.6 \text{ e}10 \text{ Pa}, \quad v_w = 200 \text{ r/min}, \quad b = 1.2 \text{ mm}, \quad \alpha = 0.8, \quad \delta_w = 1 \text{ e-}6 \text{ m}.$$

Fig 4 (a) show the online identified air-gap flux according to stator voltages and currents. Obviously, this online identify method based on  $U - I$  model is very stable and insensitive to the grinding process.



(a) Air-gap flux

(b) Vibration displacement

(c) Control current

Fig. 4 Online identified air-gap flux and vibration displacement and control current

Fig 4(b) (c) is grinding wheel's vibration displacement and control currents in control windings at  $x, y$  axis and at  $\Omega = 6000r / \text{min}$ . The vibration displacement has been a little offset upward due to the grinding force and vibration displacement is symmetrical about horizontal coordination in  $y$  direction from Fig 4(b), Fig 4(c) shows that the control currents is to stabilize soon. Fig 4(b) proved that the control scheme has an obvious effect on unbalanced vibration, about to 30 ~ 40% .

### Summary

To effectively control unbalanced vibration caused by grinding wheel mass unbalance, a new active control strategy for grinding wheel unbalanced vibration is proposed. The radial electromagnetic control force model of induction motor with dual windings and the model of force exerted on the grinding wheel are given, and then the dynamic model of flexible induction spindle-grinding wheel is constructed by finite element method, the active control scheme is designed and simulated. The results show that the scheme proposed in this paper has good performance on suppressing the unbalanced vibration.

### References

- [1] M. Xiao, S. Karube, T. Soutome, K. Sato: International Journal of Machine Tools & Manufacture Vol. 42(2002), p.1677–1685.
- [2] Han J G, Wang G C: Journal of Xuzhou Normal University (Natural Science Edition Vol.25(2007), p.65-68.
- [3] Yu T B, Gong Y D, Liang S: International Conference on Smart Materials and Nanotechnology in Engineering, Proc. of SPIE .6423(2007) Y 4231.
- [4] Nian H, He Y K: Proceedings of The Chinese Society Vol.23(2003), p.139-144.
- [5] Lv L, Xiong W L, Huang H W, Cai H X: Precise Manufacturing & Automation Vol.126(2006), p.13-16.
- [6] Y.S. Chen, Y.D. Cheng, J.J. Liao, C.C. Chiou: Finite Elements in Analysis and Design Vol.44 (2008), p.483 – 492.
- [7] Cai G Y, Huang S D: Electric Machines and Control Vol.11(2007), p.116-124.

# A Theoretical Model for Calculating Vibration Characteristics of A Kind of Driver Seat with Air Spring and MR Damper

Zhu Xingxing<sup>1, a</sup>, Zhu Sihong<sup>2, b</sup>

<sup>1</sup> 220 Mailbox, 40th, Dianjiangtai Road, Pukou, Nanjing, 210031, China

<sup>2</sup> Mechanical engineering dept, Nanjing Agricultural University, 210031, China

<sup>a</sup>zxxcomeon@yahoo.cn, <sup>b</sup>zhushihong@njau.edu.cn

**Key words:** Air spring; MR damper; Auxiliary chamber; Equivalent stiffness; Equivalent damping

**Abstract.** In order to further reduce the vibration transmitted from vehicle to driver, a new model of driver scissors linkage seat suspension was put forward, in which an air spring with auxiliary chamber and a MR damper are between the face and floor of the seat. The motion differential equation of this seat suspension system was established and the theoretical computing formulation of its equivalent vertical stiffness, equivalent damping coefficient, natural frequency and damping rate were deduced. Besides, taking HY-Z04 scissors linkage seat, SK37-6 air spring of ContiTech and RD-1005-3 MR damper of LORD as an example, the equivalent stiffness and damping coefficient in different conditions of the air spring pressure, the sprung mass, the orifice diameter and MR damping were computed and analyzed. The study results show that the air spring pressure, the sprung mass, the orifice diameter and MR damping all have obvious influence on the equivalent stiffness and damping coefficient, so the seat comfort can be improved by changing the air spring pressure, the orifice diameter and MR damping according to driver's weight and road condition.

## Nomenclature

- $\alpha$  angle between the linkage and the floor of the seat;
- $\theta$  angle between MR damper and the floor of the seat;
- $k_a$  stiffness caused by effective area changes of air spring, N/m;
- $k_v$  stiffness caused by effective volume changes of air spring, N/m;
- $V_s$  effective volume of air spring, m<sup>3</sup>;
- $V_a$  effective volume of auxiliary chamber in static equilibrium position, m<sup>3</sup>;
- $V_{s0}$  effective volume of air spring in static equilibrium position, m<sup>3</sup>;
- $A_e$  effective cross-sectional area of air spring in static equilibrium position, m<sup>2</sup>;
- $\rho_0$  air density of air spring in static equilibrium position, kg/m<sup>3</sup>;
- $n$  volume ratio of main chamber and auxiliary chamber in static equilibrium position;
- $\gamma$  changing ratio of effective cross-sectional area to spring height in micro-vibration;
- $\beta$  changing ratio of volume to spring height in micro-vibration;
- $d_0$  the orifice diameter, m;
- $f_d$  sliding friction coefficient;
- $c_e$  equivalent damping coefficient of the air spring with auxiliary chamber, N·s/m;
- $c_1, c_0$  damping coefficient of MR damper, damping coefficient of the orifice, N·s/m;
- $\mu, k$  flow corrected coefficient of orifice, adiabatic exponent;
- $l_1, l_2$  distance between O and A, distance between O and C, m;
- $L, l_3$  overall length of linkage, horizontal distance between O and the upper end of air spring, m;
- $f_1, \omega$  excitation frequency, circular frequency of excitation,  $\omega=2\pi f_1$ ;
- $P_{s0}, P_0$  air spring pressure in static equilibrium position, standard atmospheric pressure, Pa;

## Introduction

Scissors linkage seats, in which scissors linkage is used as the supporting and guiding mechanism, have been widely used in many kinds of vehicles because of its good stability and high reliability [1]. In order to further reduce the vibration transmitted from vehicle to driver, a valid way is to adopt

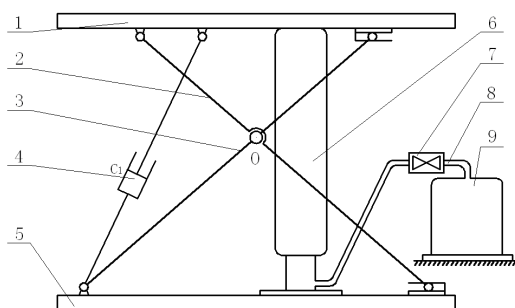
adjustable spring- damper-element, which can adjust stiffness and damping coefficient according to work condition of vehicle in time [2]. MR damper and the air spring with auxiliary chamber is such spring damper element, that widely used in practice.

Based on MR damper, Load developed a semi-active seat suspension system—MotionMaster, which can effectively reduce 40% of vibration and 49% of impact in laboratory tests [3]. Grammer developed a driver seat based on air spring with auxiliary chamber [4], in which the electrical control unit controlled throttle valve opening according to the feedback signal of response displacement and response acceleration to regulate the natural frequency of suspension system to avoid resonance of the driver seat. Zhu Sihong, Xu xiaomei [5] researched the dynamic characteristic of a scissors linkage seat, in which the spring was placed horizontally between the two scissors linkages and the damper was placed tipsily between the face and floor of the scissors linkage seat. Besides, a theoretical medel for calculating equivalent stiffness and equivalent damping was developed. Zhu Sihong, Wang minna [6] established a theoretical model of the seat suspension with air spring and damper, in which the air spring was placed vertically between the jointed point of two scissors linkages and the floor of the seat, and the damper was also placed tipsily between the face and floor of the scissors linkage seat.

The motion differential equation of the seat suspension system of a scissors linkage seat was established, in which the air spring with auxiliary chamber and MR damper are between the face and floor of the seat, and the theoretical computing formulation of it's equivalent vertical stiffness, equivalent damping coefficient, natural frequency and damping rate were deducted. Besides, the equivalent stiffness, damping coefficient in different conditions of the air spring pressure, the sprung mass, the orifice diameter and MR damping were analyzed based on an example.

**Establishment of the theoretical model**

**Suspension System for the Drive Seat.**



1 Seat 2, 3 Scissors linkages 4 MR damper 5 Seat bottom 6 Air spring 7 Proportional valves

Fig.1 Structure diagram of seat suspension system

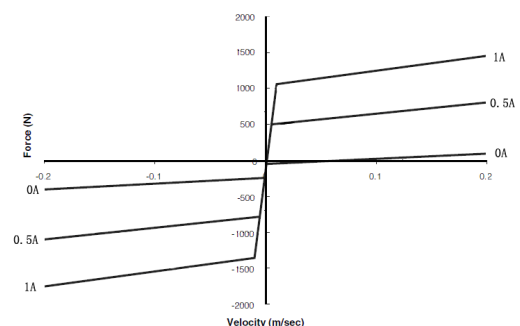


Fig.2 Force-velocity hysteresis curve of MR damper (RD-1005-3)

RD-1005-3 produced by LORD Company is selected as damping element, whose characteristic curve is shown in Fig.2. The air spring SZ35-11 produced by ContiTech Company is selected as elastic element, whose characteristic curve is shown in Fig.3. A auxiliary volume is added to enlarge the volume of the air spring which is connected with the air spring by tube with a proportional valve.

**Establishment of motion differential equation.** It is assumed that the seat vibrates in the static equilibrium position and the vibrating amplitude is small. The mass of the scissors linkages and the friction in joints are ignored. In order to derive the motion differential equation, the seat is divided into three free bodies. The corresponding force diagrams can be drawn as in Fig.4 and Fig.5.

Linkages As shown in Fig.4 and Fig.5,  $F_{d1}$ ,  $F_{d2}$  and  $F_k$  are the damping force of MR damper, the air spring with auxiliary chamber and the elastic force of the air spring;  $F_{ax}$ ,  $F_{ay}$ ,  $F_{cx}$ ,  $F_{cy}$ ,  $F_{ox}$ ,  $F_{oy}$  and  $F_{bx}$ ,  $F_{by}$ ,  $F_{dx}$ ,  $F_{dy}$  represent the forces in joints A, C, O, O' and in Slide B and D;  $y_s$  and  $\dot{y}_s$  are the displacement and velocity of the harmonic excitation acting on the seat bottom, and  $y$ ,  $\dot{y}$  and  $\ddot{y}$  represent the displacement, velocity and acceleration of the seat where  $y_s = U \sin \omega t$ ;  $I_1$ ,  $I_2$ ,  $I_3$

and  $L$  are the distance between  $O$  and  $A$ , the distance between  $O$  and  $C$ , the horizontal distance between  $O$  and the air spring and the length of the scissors linkage;  $\alpha$  and  $\theta$  are the angles between the scissors linkage and MR damper and the seat bottom in static equilibrium position;  $c_1$  and  $c_e$  represent the damping coefficient of MR damper and the damping coefficient of the air spring with auxiliary chamber,  $f_d$  is the sliding friction coefficient.

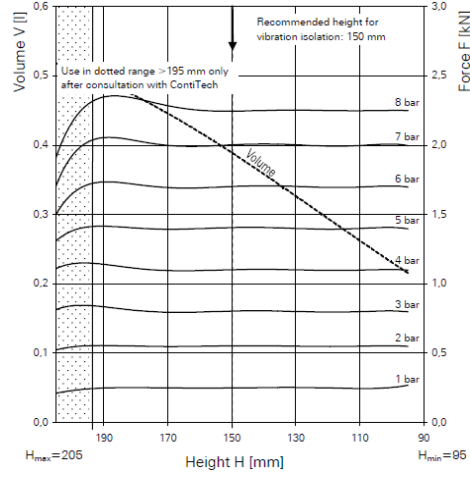


Fig.3 The relationship curve between load and displacement of the type SZ35-11's air spring

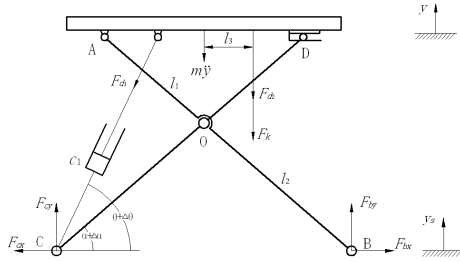


Fig.4 Forces acting on the seat suspension

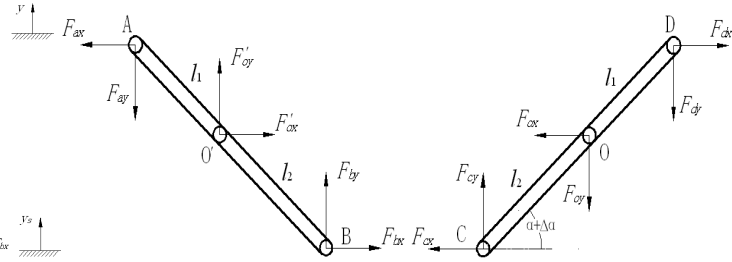


Fig.5 Forces acting on the scissors

The balance equations of the seat system can be established using the Alembert Principle. To the whole seat:

$$\sum X = 0, \quad -F_{cx} + F_{bx} - F_{d1} \cos(\theta + \Delta\theta) = 0 \quad (1)$$

$$\sum Y = 0, \quad F_{cy} + F_{by} - m\ddot{y} - F_{d1} \sin(\theta + \Delta\theta) - F_{d2} - F_k = 0 \quad (2)$$

$$\sum M_C = 0, \quad 2F_{by}l_2 \cos(\alpha + \Delta\alpha) - (F_{d2} + F_k)(l_2 \cos \alpha + l_3) - m\ddot{y}l_2 \cos(\alpha + \Delta\alpha) = 0 \quad (3)$$

To scissors linkage AB:

$$\sum X = 0, \quad F'_{ax} - F_{ax} + F_{bx} = 0 \quad (4)$$

$$\sum Y = 0, \quad F'_{ay} - F_{ay} + F_{by} = 0 \quad (5)$$

$$\sum M_O = 0, \quad F_{ax}l_1 \sin \alpha + F_{ay}l_1 \cos \alpha + F_{by}l_2 \cos \alpha + F_{bx}l_2 \sin \alpha = 0 \quad (6)$$

To scissors linkage CD:

$$\sum X = 0, \quad -F_{cx} + F_{dx} - F_{ax} = 0 \quad (7)$$

$$\sum Y = 0, \quad F_{cy} - F_{dy} - F_{ay} = 0 \quad (8)$$

$$\sum M_O = 0, \quad F_{cx}l_2 \sin \alpha + F_{cy}l_2 \cos \alpha + F_{dx}l_1 \sin \alpha + F_{dy}l_1 \cos \alpha = 0 \quad (9)$$

with

$$F_{d1} = c_1(\dot{y} - \dot{y}_s) \cdot \sin \theta \quad F_{d2} = c_e(\dot{y} - \dot{y}_s) \quad F_k = k_e(y - y_s) \quad F_{bx} = f_d F_{by} \quad F_{dx} = f_d F_{dy} \quad L = l_1 + l_2$$

By solving equations (1) ~ (9) and introducing equations  $\alpha + \Delta\alpha \approx \alpha$  and  $\theta + \Delta\theta \approx \theta$  (when the vibrating amplitude is small), the motion differential equation is deduced:

$$\begin{aligned} & \ddot{y} + \left\{ \left[ 1 + \frac{2l_3 f_d \sin \alpha}{(f_d \sin \alpha + \cos \alpha)L \cdot \cos \alpha} \right] \frac{c_e}{m} + \left[ \frac{l_2 (\cos \alpha - f_d \sin \alpha) \sin(\theta - \alpha) \sin \theta}{L(f_d \sin \alpha + \cos \alpha) \cos \alpha} + \frac{l_1 \sin(\theta + \alpha) \sin \theta}{L \cos \alpha} \right] \frac{c_1}{m} \right\} \dot{y} \\ & + \left[ 1 + \frac{2l_3 f_d \sin \alpha}{(f_d \sin \alpha + \cos \alpha)L \cdot \cos \alpha} \right] \frac{k_e}{m} y \\ & = \left\{ \left[ 1 + \frac{2l_3 f_d \sin \alpha}{(f_d \sin \alpha + \cos \alpha)L \cdot \cos \alpha} \right] \frac{c_e}{m} + \left[ \frac{l_2 (\cos \alpha - f_d \sin \alpha) \sin(\theta - \alpha) \sin \theta}{L(f_d \sin \alpha + \cos \alpha) \cos \alpha} + \frac{l_1 \sin(\theta + \alpha) \sin \theta}{L \cos \alpha} \right] \frac{c_1}{m} \right\} \dot{y}_s \\ & + \left[ 1 + \frac{2l_3 f_d \sin \alpha}{(f_d \sin \alpha + \cos \alpha)L \cdot \cos \alpha} \right] \frac{k_e}{m} y_s \end{aligned} \tag{10}$$

Generally, the air spring with auxiliary chamber is non-linear. According Wang's suggestion, it can be simplified to a linear system when the vibrating amplitude is small. Its stiffness and damping characteristic can be described with equivalent stiffness  $k_e$  and equivalent damping  $c_e$ . The theoretical formulas for calculating  $k_e$  and  $c_e$  are as follows [7]:

$$k_e = \frac{[nk_v^2 + (1+n)k_v k_a][ (1+n)k_v ]}{[(1+n)k_v]^2 + (\omega c_0)^2} + \frac{c_0^2 (k_v + k_a) \omega^2}{[(1+n)k_v]^2 + (\omega c_0)^2} \tag{11}$$

$$c_e = \frac{c_0 k_v^2}{[(1+n)k_v]^2 + (\omega c_0)^2} \tag{12}$$

Where  $k_v = \gamma \frac{kP_{s0} A_{e0}}{V_{s0}}$   $k_a = -\beta(P_{s0} - P_0)$   $\gamma = \frac{\Delta V_s}{\Delta h}$   $\beta = \frac{\Delta A_e}{\Delta h}$   $n = V_{s0} / V_a$   $c_0 = \gamma \rho_0 \mu A_{e0} / d_0^3$

$h$ ,  $V_a$ ,  $A_e$  and  $V_{s0}$  are the air spring height, the volume of the auxiliary chamber, the effective cross-sectional area and effective volume of the air spring in static equilibrium position;  $n$ ,  $\gamma$ ,  $\beta$ ,  $k_a$  and  $k_v$  represent the volume ratio of the air spring and the auxiliary chamber in static equilibrium position, the changing ratio of  $A_e$  and  $V_{s0}$  to spring height in small vibrating amplitude, the stiffness caused by  $A_e$  and  $V_{s0}$  changes;  $P_0$ ,  $P_{s0}$  and  $\rho_0$  are the standard atmospheric pressure, the air spring pressure and the air density in the air spring in static equilibrium position;  $k$ ,  $d_0$ ,  $c_0$  and  $\mu$  represent the adiabatic index of the air, the orifice diameter, the damping coefficient and the flow corrected coefficient of the orifice;  $\omega$  and  $f_1$  are the circular frequency and the frequency of the harmonic excitation, where  $\omega = 2\pi f_1$ .

Substituting equations (11) and (12) in equations (10), the motion differential equation of the seat suspension is obtained:

$$\begin{aligned} & \ddot{y} + \left\{ \left[ 1 + \frac{2l_3 f_d \sin \alpha}{(f_d \sin \alpha + \cos \alpha)L \cdot \cos \alpha} \right] \frac{c_0 k_v^2}{m[(1+n)k_v]^2 + m(\omega c_0)^2} + \left[ \frac{l_2 (\cos \alpha - f_d \sin \alpha) \sin(\theta - \alpha) \sin \theta}{L(f_d \sin \alpha + \cos \alpha) \cos \alpha} \right. \right. \\ & \left. \left. + \frac{l_1 \sin(\theta + \alpha) \sin \theta}{L \cos \alpha} \right] \frac{c_1}{m} \right\} \dot{y} + \left[ 1 + \frac{2l_3 f_d \sin \alpha}{(f_d \sin \alpha + \cos \alpha)L \cdot \cos \alpha} \right] \frac{[nk_v^2 + (1+n)k_v k_a][ (1+n)k_v ] + c_0^2 (k_v + k_a) \omega^2}{m[(1+n)k_v]^2 + m(\omega c_0)^2} y \\ & = \left\{ \left[ 1 + \frac{2l_3 f_d \sin \alpha}{(f_d \sin \alpha + \cos \alpha)L \cdot \cos \alpha} \right] \frac{c_0 k_v^2}{m[(1+n)k_v]^2 + m(\omega c_0)^2} + \left[ \frac{l_2 (\cos \alpha - f_d \sin \alpha) \sin(\theta - \alpha) \sin \theta}{L(f_d \sin \alpha + \cos \alpha) \cos \alpha} \right. \right. \\ & \left. \left. + \frac{l_1 \sin(\theta + \alpha) \sin \theta}{L \cos \alpha} \right] \frac{c_1}{m} \right\} \dot{y}_s + \left[ 1 + \frac{2l_3 f_d \sin \alpha}{(f_d \sin \alpha + \cos \alpha)L \cdot \cos \alpha} \right] \frac{[nk_v^2 + (1+n)k_v k_a][ (1+n)k_v ] + c_0^2 (k_v + k_a) \omega^2}{m[(1+n)k_v]^2 + m(\omega c_0)^2} y_s \end{aligned} \tag{13}$$

**Vibration characteristics of the seat suspension system.** The equivalent stiffness  $k_s$  and the equivalent damping coefficient  $c_s$  as well as the equivalent damping rate  $\zeta$  of the seat suspension can be obtained from equation (13):

$$k_s = m\omega_0^2 = \left[1 + \frac{2l_3 f_d \sin \alpha}{(f_d \sin \alpha + \cos \alpha)L \cdot \cos \alpha}\right] \cdot \frac{[nk_v^2 + (1+n)k_v k_a][[(1+n)k_v] + c_0^2(k_v + k_a)\omega^2]}{[(1+n)k_v]^2 + (\omega c_0)^2} \quad (14)$$

$$c_s = \left[1 + \frac{2l_3 f_d \sin \alpha}{(f_d \sin \alpha + \cos \alpha)L \cdot \cos \alpha}\right] \frac{c_0 k_v^2}{[(1+n)k_v]^2 + (\omega c_0)^2} + \left[\frac{l_1 \sin(\theta + \alpha) \sin \theta}{L \cos \alpha} + \frac{l_2 (\cos \alpha - f_d \sin \alpha) \sin(\theta - \alpha) \sin \theta}{L(f_d \sin \alpha + \cos \alpha) \cos \alpha}\right] c_1 \quad (15)$$

$$\zeta = \frac{c_s}{2m\omega_0} = \frac{\left[1 + \frac{2l_3 f_d \sin \alpha}{(f_d \sin \alpha + \cos \alpha)L \cdot \cos \alpha}\right] \frac{c_0 k_v^2}{[(1+n)k_v]^2 + (\omega c_0)^2} + \left[\frac{l_2 (\cos \alpha - f_d \sin \alpha) \sin(\theta - \alpha) \sin \theta}{L(f_d \sin \alpha + \cos \alpha) \cos \alpha} + \frac{l_1 \sin(\theta + \alpha) \sin \theta}{L \cos \alpha}\right] c_1}{2m \sqrt{\left[1 + \frac{2l_3 f_d \sin \alpha}{(f_d \sin \alpha + \cos \alpha)L \cdot \cos \alpha}\right] \frac{[nk_v^2 + (1+n)k_v k_a][[(1+n)k_v] + c_0^2(k_v + k_a)\omega^2]}{m[(1+n)k_v]^2 + m(\omega c_0)^2}}} \quad (16)$$

It is easily to obtain the natural frequency  $f_0$ :

$$f_0 = \frac{\omega_0}{2\pi} = \frac{1}{2\pi} \sqrt{\left[1 + \frac{2l_3 f_d \sin \alpha}{(f_d \sin \alpha + \cos \alpha)L \cdot \cos \alpha}\right] \frac{[nk_v^2 + (1+n)k_v k_a][[(1+n)k_v] + c_0^2(k_v + k_a)\omega^2]}{m[(1+n)k_v]^2 + m(\omega c_0)^2}} \quad (17)$$

From equations (14) ~ (17), it can be seen that  $k_s, f_0, c_s$  and  $\zeta$  are effected by  $w, c_1, c_0, \alpha, \theta, l_1, l_2, l_3, L, k_a, k_v, m, f_d$  and  $n$ .

### Example

**Parameters of seat suspension system.** The standard atmospheric pressure (0.101MPa) and standard temperature (293K) are taken as the external work environment. The equivalent sprung mass on the seat suspension system is supposed to be 55 kg to 95 kg [8], and the equilibrium position by 65kg equivalent sprung mass is chosen as the initial position approximately. The HY-Z04 scissors linkage seat is chosen as example, the SZ35-11 air spring produced by ContiTech Company and LORD's RD-1005-3 MR damper are respectively selected as elasticity and damping elements. The corresponding geometric and physic parameters in initial position are shown in Table 1, where  $fd=0.02$  is friction coefficient between slide couples.

Table 1 **Geometric** and physic parameters of seat suspension system

$L/m$	$l_1/m$	$l_2/m$	$f_d$	$\theta/^\circ$	$\alpha/^\circ$	$h_0/mm$	$V_{s0}/m^3$	$V_{a0}/m^3$	$\gamma$	$\beta$	$k$	$\mu$
0.245	0.102	0.143	0.02	21.6	11.2	150	0.00038	0.00076	0.0031	-0.03	1.4	0.03

According to research results in literature [9] and [6], the volume ratio of auxiliary chamber and main chamber is taken as 0.5 and the orifice diameter is selected as 0mm ~ 5mm.  $k_v, k_a$  and  $c_0$  can be calculated by using equations (13) and parameters in Table 1. The equivalent sprung mass is divided into three groups: 55~65kg, 70~85kg and 90~95kg, corresponding to the air spring pressure 0.3MPa, 0.4MPa and 0.5MPa. Table 2 shows values of  $P_{s0}, A_{e0}$  and  $\rho_0$  related to different  $m$ .

Table 2 Values of  $P_{s0}, A_{e0}$  und  $\rho_0$  related to different  $m$

$m /kg$	65	80	95
$P_{s0}/MPa$	0.3	0.4	0.5
$A_{e0}/m^2$	0.00267	0.00275	0.0028
$\rho_0/kg/m^3$	3.654	4.872	6.09

Damping coefficients of MR damper corresponding to different input currents 0, 0.25, 0.5, 0.75 and 1A are calculated according to the hysteresis characteristics curve in Fig.2. They are 714.28 N.s/m, 1120.74 N.s/m, 1473 N.s/m, 1771 N.s/m and 2015 N.s/m.

**Calculating results and analysis.** By substituting parameters from tables 1 and 2 in equations (15) and (16), it is easy to obtain the value of equivalent stiffness and damping coefficient changing with the orifice diameter, the air spring pressure, the sprung mass and the input current of MR damper.

Figure 6 shows that the equivalent stiffness and damping coefficient of the system change with the orifice diameter and the input current of MR damper by different air spring pressure and equivalent sprung mass. As shown in the figures 6 (a), (c) and (e),  $k_s$  increases with the air spring pressure increasing and the input current of MR damper has little effect on it. For each air spring pressure,  $k_s$  keeps constant essentially when the orifice diameter is less than  $\Phi 1\text{mm}$  and greater than  $\Phi 3\text{mm}$ , while it decreases rapidly when the orifice diameter is between  $\Phi 1\text{mm}$  and  $\Phi 3\text{mm}$ . It means that  $d = \Phi 1\text{mm} \sim \Phi 3\text{mm}$  is the ‘sensitive zone’ of system’s equivalent stiffness.

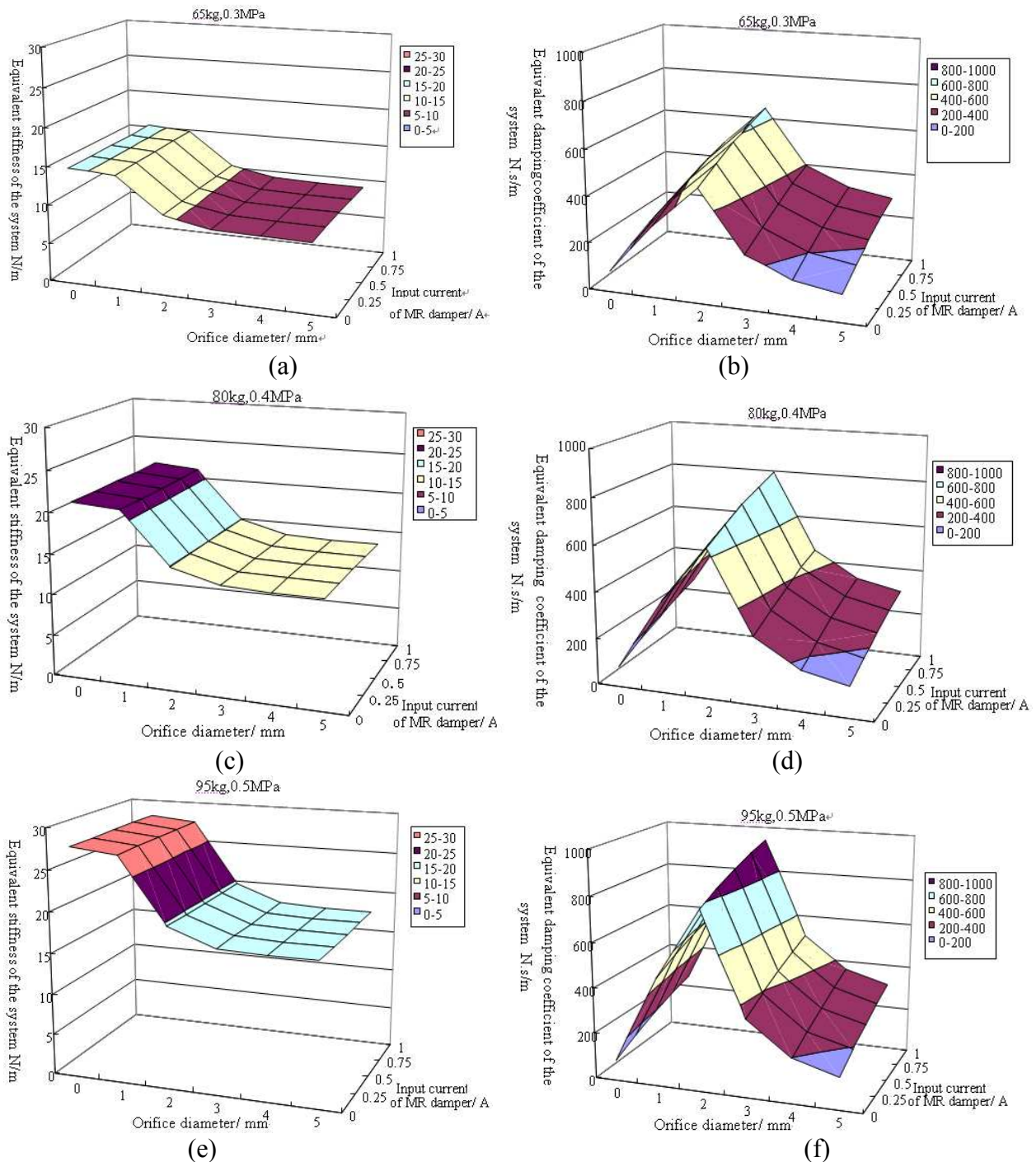


Fig.6 The effect of the orifice diameter and the input current of MR damper on the equivalent stiffness and damping coefficient

Figures 6 (b), (d) and (f) show that the equivalent damping coefficient  $c_s$  increases with the air spring pressure and input current increasing. For each air spring pressure, with the orifice diameter increasing,  $c_s$  increases first and reaches to maximum by  $d \approx \Phi 2\text{mm}$ , and then decreases until it reaches steady value by  $d \approx \Phi 5\text{mm}$  which is about the same for different air spring pressure. When the orifice diameter is greater than  $\Phi 5\text{mm}$ , it has almost no influence on the equivalent damping coefficient.

### Conclusions

A theoretical model for calculating the equivalent stiffness and damping coefficient of a kind of driver seat with air spring with auxiliary chamber and MR damper was established (equations (14) and (15)). Taking HY-Z04 scissors linkage seat as example, the effect of the air spring pressure, the sprung mass, the orifice diameter and the input current of MR damper on the equivalent stiffness and damping coefficient of the system was analyzed. The research shows that the theoretical model can be used to select air spring with auxiliary chamber and MR damper by the design of scissors linkage driver seat.

### References

- [1] H.J. Matthies, F.Meier, Jahrbuch Agrartechnik, Landwirtschaftsverlag (1999) 21-24.
- [2] S.B. Choi, Y.M Han, Vibration control of electrorheological seat suspension with human-body model using sliding mode control, Journal of Sound and Vibration 303 (2007) 391-404.
- [3] J. Wu, H.F. Wang: Mechanical & Electrical Engineering Magazine in China Vol.25 (2008), p. 74-76.
- [4] L.D. Daniel, E.S. Troy, John Deere active seat: a new level of seat performance, Agricultural Engineering (2002) 02-IE-002.
- [5] X.M. Xu, S.H. Zhu: China Mechanical Engineering Vol.17 (2006), p.802-804.
- [6] M.N. Wang: Research on vibration characteristic of scissors linkage seat with suspension of the air spring with auxiliary chamber, Nanjing Agricultural University in China (2008).
- [7] J.S. Wang, S.H. Zhu, L. He: China Mechanical Engineering Vol.12 (2009), p.1418-1421.
- [8] X.M. Xu, Researches on driver seat suspension system of off-road vehicles based on magnetic spring, Nanjing Agricultural University in China (2006).
- [9] J.S. Wang, Researches on dynamic characteristics of air spring with auxiliary chamber, Nanjing Agricultural University in China (2009).

## Aeroengine Oil Fault Diagnosis based on D-S Evidential Theory

Qu hongchun<sup>1, 2, a</sup>, Ding xiebin<sup>2, b</sup> and Wang taiyong<sup>1</sup>

<sup>1</sup> School of Mechanical Engineering, Tianjin University, Tianjin,300070, P.R.China

<sup>2</sup> College of Aeronautical Engineering, Civil Aviation University of China, Tianjin,300300, P.R.China

<sup>a</sup>qhc@eyou.com, <sup>b</sup>weylby@126.com

**Keywords:** Aerospace Propulsion theory and Engineering; wear debris; Dempster-Shafer evidence combination; fault diagnosis

**Abstract.** Aeroengine oil contains wear debris generated by friction. Based on the Dempster-Shafer evidence combination theory, aeroengine wear conditions can be effectively diagnosed. Through analysing the elements of wear debris in lubricating medium, it can determine engines wear levels and wear parts, as references for troubleshooting. In the process of combination, an method was proposed that every element of wear quantity and wear rate were fused at first, then the integration of all elements. For Dempster-Shafer has its own limitations, two improved methods were applied to and were compared. The results show that Dempster-Shafer evidence combination is an effective fault diagnosis method for aeroengine oil wear condition.

### Intorduction

Aeroengine is the kernel power supply of aircraft, whose structure is complex and operation environment is very hard, so it is the main source of aircraft faults, and its condition is the direct influencing factor of flight safty and airline company benefit. According to ICAO's statistics, the ratio of mechanical failure in all accidents is generally 25% to 30%. In various types of air accidents caused by many mechanical factors, the aeroengine is the key factor, and wear fault is a extremely important failure mode in the lots of engine failure[1]. With the improved performance of the aeroengines, the components working conditions are becoming worse and worse. The consumption of the engine oil and partly high metal contents in the oil are reflecting the wear condition of bearing, casing and gear. Through analyzing the elements wear quantity in the oil, it can conclude whether there has wear fault of aeroengine or not and access the the severity of fault. It provides favorable and reliability references for reducing unnecessary components replacement, reduceing secondary injury and developing the most effective and economical maintenance program.

### The dempster-shafer theory of evidence

**Dempster-Shafer Theory [2].** The Dempster-Shafer theory is a mathematical theory of evidence; it is a powerful tool for combining measures of evidences.

Frame of discernment: Let  $\Theta$  be a finite set of elements, an element can be a hypothesis, an object, or in our case a fault. We refer to  $\Theta$  as the frame of discernment. The set consisting of all the subsets of  $\Theta$  is called the power set of  $\Theta$ , and denoted by  $\Omega(\Theta)$ . As an example, suppose that an engine may suffer from one or more of three faults a, b and c. The frame of discernment in this case can be set as:  $\Theta = \{a, b, c\}$  and  $\Omega(\Theta) = \{\Phi, \{a\}, \{b\}, \{c\}, \{a, b\}, \{a, c\}, \{b, c\}, \{a, b, c\}\}$

Mass functions: When the frame of discernment is determined, the mass function  $m$  is defined as a mapping of the power set  $\Omega(\Theta)$  to a number between 0 and 1, i.e,

$$m(\emptyset) = 0, \sum_{A \subseteq \Theta} m(A) = 1 \quad (1)$$

Where,  $m$  is called a basic probability assignment function.  $m(A)$  expresses the proportion of all relevant and evidence that supports the claim that a particular element of  $\Theta$  belongs to the set  $A$ .

Belief and Plausibility functions: The belief function  $Bel$  is defined as

$$Bel: \Omega(\Theta) \rightarrow [0,1] \text{ and } Bel(B) = \sum_{A \subseteq B} m(A) \quad (2)$$

The plausibility function  $Pls$  is defined as:

$$Pls: \Omega(\Theta) \rightarrow [0,1] \text{ and } Pl(B) = 1 - Bel(\bar{B}) \quad (3)$$

The belief function  $Bel(B)$  measures the total amount of probability that must be distributed among the elements of  $A$ ; it reflects inevitability and signifies the total degree of belief of  $A$  and constitutes a lower limit function on the probability of  $B$ . On the other hand, the plausibility function  $Pls(B)$  measures the maximal amount of probability that can be distributed among the elements in  $B$ ; it describes the total belief degree related to  $B$  and constitutes an upper limit function on the probability of  $B$ .  $Bel(B)$  and  $Pls(B)$  are shown on Fig.1

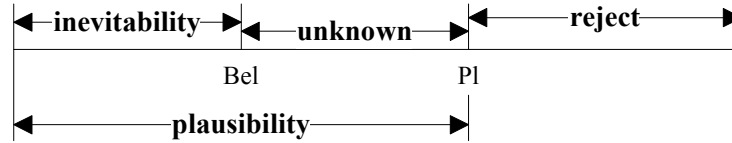


Fig.1 Belief and Plausibility functions

**Rules of evidence combination.** Suppose  $m_1$  and  $m_2$  are two mass functions formed based on information obtained from two different information sources in two frames of discernment  $H_1$  and  $H_2$ ; Let  $A_i$  and  $B_j$  be focal elements of  $Bel_1$  and  $Bel_2$  respectively, where  $i = 1, \dots, n$  and  $j=1, \dots, n$ ,  $\sum_{A_i \cap B_j = \emptyset} m_1(A_i)m_2(B_j) < 1$ , according to Dempster-Shafer's orthogonal rule we have:

$$m(C) = \begin{cases} \frac{\sum_{A_i \cap B_j = C} m_1(A_i)m_2(B_j)}{1 - \sum_{A_i \cap B_j = \emptyset} m_1(A_i)m_2(B_j)} & C \neq \emptyset \\ 0 & C = \emptyset \end{cases} \quad (4)$$

Generally, for  $n$  mass functions,  $m_1, m_2, \dots, m_n$  in  $\Theta$ , the mass function after combination is:

$$m(C) = \begin{cases} \frac{\sum_{\cap A_i = C} \prod_{1 \leq i \leq N} m_i(A_i)}{1 - \sum_{\cap A_i = \emptyset} \prod_{1 \leq i \leq N} m_i(A_i)} & C \neq \emptyset \\ 0 & C = \emptyset \end{cases} \quad (5)$$

**The example of combination.** There are two mass functions,  $\Theta = \{A, B, C\}$  as following:

$$m_1(\theta) = \begin{cases} 0.9 & \theta = A \\ 0.1 & \theta = B \\ 0 & \theta = C \end{cases}, m_2(\theta) = \begin{cases} 0 & \theta = A \\ 0.1 & \theta = B \\ 0.9 & \theta = C \end{cases}. \quad (6)$$

Applying the principles of Evidence Theory, we can conclude that:  $m(B) = 1$ , Although the two pieces of evidence are reluctant to support  $B$ , the synthetic result is absolutely support  $B$  for the true proposition. Obviously, it is inconsistent with common sense. Thus Murphy [4] proposed a combination rule theory of the conflict evidences. And Wang [3] has been improved it, called the weighted distribution method.

### The improved rules of evidence combination

**Weighted Distribution method.** Suppose  $H_1$  and  $H_2$  are two evidences formed in the frames of discernment  $\Theta$ ,  $m_1$  and  $m_2$  are two mass functions.  $H_1$  and  $H_2$ ;  $A_i \subseteq H_1$  and  $B_j \subseteq H_2$ , the similarity coefficient of two evidences is:

$$d_{12} = \frac{\sum_{A_i \cap B_j = C_k} m_1(A_i)m_2(B_j)}{\sqrt{(\sum m_1^2(A_i))(\sum m_2^2(B_j))}} \quad (7)$$

Similarity matrix:

$$S = \begin{bmatrix} 1 & d_{12} & \dots & d_{1n} \\ d_{21} & 1 & \dots & d_{2n} \\ \vdots & \vdots & \ddots & \vdots \\ d_{n1} & d_{n2} & \dots & 1 \end{bmatrix} \quad (8)$$

Support for evidences:

$$\text{sup}(m_i) = \sum_{j=1}^n d_{ij} \quad (9)$$

Belief:

$$\text{crd}(m_i) = \frac{\sum_{j=1}^n d_{ij}}{\sum_{i=1}^n \sum_{j=1}^n d_{ij}} \quad (10)$$

Applying the principles of Weighted Distribution Evidence Theory:  $m(A) = 0.45$ ,  $m(B) = 0.1$ ,  $m(C) = 0.45$ , obviously, it is consistent with common sense.

**Quasi-Associative method.** In 1987, Yager [5] introduced an improved method, called quasi-associative.  $A \subseteq \Theta$ , the rules of combination as following:

$$m(C) = \begin{cases} 0 & C = \emptyset \\ \sum_{\cap A_i = C} \prod_{1 \leq i \leq N} m_i(A_i) & C \neq \emptyset \end{cases} \quad (11)$$

Quasi-associativity means that the operator can be broken down into associative suboperations. For better combination, Li[6] introduced an improved method based on it:

$$m(C) = \begin{cases} 0 & C = \emptyset \\ \sum_{\cap A_i = C} \prod_{1 \leq i \leq N} m_i(A_i) + f(C) & C \neq \emptyset \end{cases} \quad (12)$$

$$K = \sum_{\cap A_i = \emptyset} \prod_{1 \leq i \leq N} m_i(A_i), \quad f(C) = K * q(C) \quad (13)$$

Where,  $q(C) = \frac{1}{n} \sum_{i=1}^n m_i(C)$ ,  $n$  means  $n$  evidences,  $q(C)$  is support for every evidence. The synthetic result is:  $m(A) = 0.45$ ,  $m(B) = 0.1$ ,  $m(C) = 0.45$ .

### Case study

**Identify wear indicators.** Currently, the evaluation engine wear condition states are following: wear quantity and wear rate. There is a lot of friction in aeroengine, as a result of leading to wear, which contributes lots of wear debris to leave in engine oil. Through the analysis of the characteristics of the element's wear quantity and wear rate can monitor aeroengine wear condition. From the engineering point of view, engine wear condition can be divided into three assessment levels: normal, warning, abnormal. Wear state of normal is the engine operating conditions good; Warning means the engine can operate normally, the user should have certain attention, meanwhile adding the appropriate level of maintenance of the engine and increasing the monitoring of density; when wear state is abnormal, the engine should stop operating and take measures to maintain in time [7].

**Information fusion design.** Evidence theory information fusion, needs to select a group of independent evidences. According to the wear condition of engine components, select four elements of Fe, Cu, Pb, Al characterize wear. Get wear and wear rate through oil analysis, as evidences of evaluate engine wear condition. Engine wear conditions divide into three assessment levels: normal, warning, abnormal. The first floor fusion is every element's information of wear quantity and wear rate, through the wear of each individual element, it can determine the specific wear of engine parts, and according to wear parts and wear degree can determine the maintenance approach; The second floor fusion is the integration of all elements, from the result, we can get information of the overall engine wear condition status, so as to identify the maintenance method. It is shown on Fig 2.

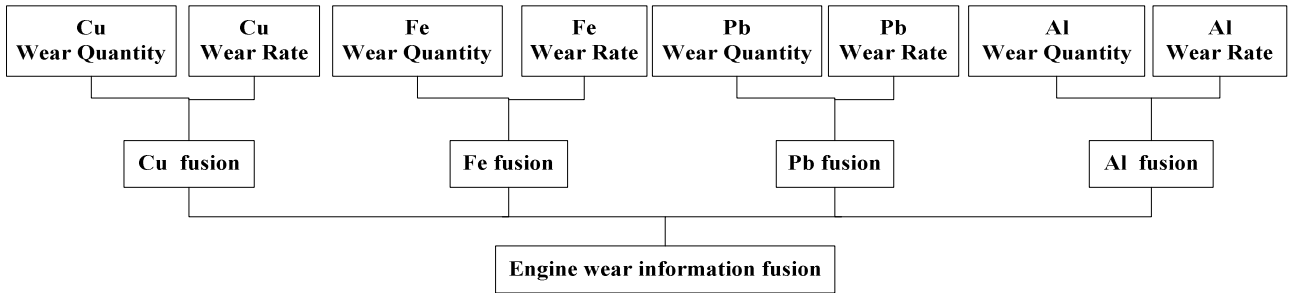


Fig.2 The Structure of engine information fusion

**Construct the frame of discernment functions.** In order to get the belief of each state, we can use experience and the statistical results to divide the engine wear range into 3: normal gradient area, warning area and the abnormal area. Considering the mean of the sample data as normal, 2 times the normal variance of the sample is a warning value, 3 times the variance is abnormal values. The limitation of aeroengine wear quantity is summarized in Tab.1 [7]; the limitation of aeroengine wear rate is summarized in Tab.2 [7].

Tab.1 The limitation of wear quantity

elements	Fe	Cu	Pb	Al
normal	0~16	0~4	0~7	0~5
warning	16~18	4~5	7~8	5~6
abnormal	18~	5~	8~	6~

Tab.2 The limitation of wear rate

elements	Fe	Cu	Pb	Al
normal	0~0.3	0~0.1	0~0.1	0~0.1
warning	0.3~0.5	0.1~0.2	0.1~0.2	0.1~0.3
abnormal	0.5~	0.2~	0.2~	0.3~

With a bell-shaped function to calculate the probability distribution, so as to determine the probability distribution functions.

For the normal probability distribution function:

$$F(x) = \begin{cases} 1 & x \leq \frac{b}{2} \\ 1 - \frac{1}{1 + \left| \frac{x-b}{p-b} \right|^c} & \frac{b}{2} < x < b \\ 0 & x \geq b \end{cases} \quad (14)$$

For the Warning state of wear failure probability distribution function:

$$F(x) = \begin{cases} 0 & x \leq \frac{b}{2} \\ \frac{1}{1 + \left| \frac{x-b}{p-b} \right|^c} & \frac{b}{2} < x \leq p \\ 0 & x > p \end{cases} \quad (15)$$

(3) For the state of abnormal probability distribution function:

$$F(x) = \begin{cases} 0 & x \leq b \\ 1 - \frac{1}{1 + \left| \frac{x-b}{p-b} \right|^c} & b < x \leq p \\ 1 & x > p \end{cases} \quad (16)$$

**Analyze the result.** Through the oil analysis, we get a simple of the four elements, it is summarized in Tab.3.

Tab.3 The simples of wear

elements	Fe	Cu	Pb	Al
Wear quantity	14.46	3.01	5.66	4.20
wear rate	0.166	0.077	0.068	0.035

Tab.4 The results of fusion

	Fe		Cu		Pb		Al		fusion
	quantity	rate	quantity	rate	quantity	rate	quantity	rate	
notmal	0.3722	0.3098	0.4950	0.0502	0.6423	0.0929	0.3902	1	
warning	0.6278	0.6902	0.5050	0.9498	0.3577	0.9071	0.6098	0	
abnotmal	0	0	0	0	0	0	0	0	
notmal	0.2012		0.0492		0.1554		0.6951		0.0056
warning	0.7988		0.9508		0.8446		0.3049		0.9944
abnormal	0		0		0		0		0

Using  $C=-2$ , we combine the information cues provided by Tab.3, we obtain the combination, the result of fusion is shown on Tab.4. For the synthesis of Al,  $m_{rate}(Al) = (1, 0, 0)$ , the evidence conflicts, applying the weighted distribution method to calculate  $m(Al) = (0.8386, 0.1614, 0)$ , applying Yager's improved formula  $m(Al) = (0.8141, 0.1859, 0)$ . In the evidence conflict annlysis, weighted distribution method and Yager's improved method have nearly the same result. Synthesis of each element is in Tab.4. Synthesis of results (A) = (0.0056, 0.9944, 0). Obviously, this diagnostic information fusion result shows that the state of the engine is a warning level, in line with the actual situation.

**Conclusions**

Applying the Dempster-Shafer evidence theory fusion method in the aeroengine wear information fusion can improve the diagnostic reliability of conclusions and reduce uncertainty. When the evidence conflicts, the application of improved methods can solve the conflicts effectively and reliability, besides, weighted distribution method and Yager's improved method have nearly the same result in the evidence conflict fusion. Thus, the Dempster-Shafer evidence theory a better integration of the engine fault diagnosis.

**Acknowledgements**

This work was financially supported by Civil Aviation University of China research fund 05yk08m and Central College Basic Scientific Research Fund ZXH2010D019.

**References**

- [1] Wu Zhenduo, Zuo Hongfu, Sun Youchao: Aviation Engineering and Maintenance Vol.4 (2000), p.25-26.
- [2] Dempster A P: Annals Mathematical Statistics Vol.38 (1967), p.325-339.
- [3] Wang Xiaoxia: *Research on the Combination Rule of Conflict Evidences* (North University of China, TaiYuan 2007), p.33-46.
- [4] Yager RR: IEEE Trans onsystem Vol.41 (1989) No.2, p.93-137.
- [5] Murphy C.K: Decision Support System (2000)
- [6] Li Bicheng,Wang Bo,Wei Jun: Journal of DataAcquisition & Processing Vol.1 (2002) No.1, p.33-36.
- [7] Fu Jianping,Zhang Peilin,Li Guozhang: Journal of Ordnance Engineering College Vol.17 (2005) No.1, p.14-16.

## Application of Generalized Stochastic Resonance to the Vibration Test

Zhang Ying<sup>1, a</sup>, Li Shu-Ming<sup>1, b</sup>

<sup>1</sup>College of Aeronautical Engineering, Civil Aviation University of China, Tianjin 300300, China

<sup>a</sup>wistaria\_kuxia@163.com

**Keywords:** Stochastic resonance; Bistable system; Generalized parameters; Signal processing; Vibration

**Abstract:** Noise, bistable system and input signal are the three essential factors in stochastic resonance (SR). The noise-induced SR method, the parameter-tuning SR method, and the twice sampling SR method change the characteristics of the noise, the bistable system and the input signal, respectively. With the new cooperation, they can all produce the SR phenomena when the system exceeds the small-parameter area. If treating the strong noise and the input signal with large frequency, the actions of the system parameters can build the system behavior in an orderly way, associated with the twice sampling frequency. The united parameter-tuning SR method adjusts the system parameters to fit the normalized frequency after the twice sampling SR, in order to make the optimal noise intensity. The application to the flow meter vibration test has presented the practicability and effectiveness of the united parameter-tuning SR method.

### Introduction

Stochastic resonance (SR) is the universal phenomenon existing in the non-linear systems, induced by the internal or external noise. It was originally proposed by Benzi [1], as an explanation of the behavior of the earth's ice ages, which exhibit a 100 000 year periodicity. In essence, SR is a nonlinear cooperative effect [1-4] in which large-scale fluctuations influence the weak periodic stimulus, leading to the result that the periodic component is greatly enhanced. There are different ways or models [2] to quantify SR in different fields. Towards different system requirements, the research and experiments have provided varied methods.

Bistable SR displays its unique advantages when dealing with the signal contaminate by the noise covering the virtual frequencies. It has been applied to detect, amplify and transmit the features or information in recent years [2-4]. The classical SR theory [5-6] was established with the condition of small parameters. It is one of the limitations in the generalization of SR technologies.

The noise-induced SR method[7], the parameter-tuning SR method[8-9] or the twice sampling method[10] induces the occurrence of the SR phenomenon in different situation. Considering the respective effect to SR, the above means can be defined as the generalized SR method. The united parameter-tuning SR method was proposed on the basis of the generalized SR theory. It was introduced to analyze the vibration of flow meter system in the following text.

### The Parameter-tuning Theory of Bistable SR

Making the bistable system as a kind of nonlinear signal processor[7], it is governed by Langevin equation

$$\frac{dx}{dt} = ax - bx^3 + s(t) + n(t). \quad (1)$$

The course can be described by the motion of a particle in the bistable system, under the influences of the driving force  $s(t) = A\sin(2\pi f_0 t)$  and the white noise  $n(t)$  with Gaussian distribution. The noise intensity is expressed as the variable  $D$ . While the signal, noise and system matching with each other properly, SR occurs and the noise's energy is transformed to enhance the signal. The ways of optimizing the different parameters influence the system behavior diversely.

**Noise-induced SR.** The noise acts on the system behavior[7]. For one thing, increasing the noise's intensity  $D$  can raise the response velocity. And then the output would be steady more quickly, along with the changes of the driving signal. For another, the stronger noise makes the output performance decline. Consequently, only with the appropriate intensity, the response velocity and the stable output are proportional to each other, the better state can be achieved. It reflects the rebuilding action of the noise [7].

**Parameter-tuning SR.** From the bistable potential  $U(x) = -1/2ax^2 + 1/4bx^4$ , we can calculate the height of the potential barrier  $U_0 = a^2/4b$ , the distance of potential wells  $\Delta x = 2\sqrt{a/b}$ , and the particle's transition speed called Kramers rate [2]

$$R_k = \frac{a}{\sqrt{2\pi}} e^{-a^2/4bD} . \quad (2)$$

The variation of the system parameters  $a$  and  $b$  cause changes in these variables [9]. It makes the relative noise energy redistribute and leads to different SR outcome. According to the regularity of the parameter choice for SR, the optimal SR can be obtained. After a scale transformation, the conventional way of adding noise can be viewed as a specific case of the method of tuning system parameters [8]. When the systems are adjustable, tuning system parameters is more practical than adding noise to the nonlinear systems. It is also applicable to the case that the noise is too heavy to play the constructive role.

**Twice sampling SR.** To make out the response to the driving force with the large frequency when SR occurs, the strategy of twice sampling SR was proposed [10]. It utilizes the energy transfer mechanism from high-frequency area to low-frequency area, by selecting the twice sampling frequency  $f_{sr}$ . The method is aiming to postpone the large frequency signal to satisfy the condition of the small parameter SR. The transformation of the driving frequency  $f_0$  is the normalized frequency  $f'_0$ , which is fit for the noise intensity  $D$ .

### Generalized stochastic resonance theory and united parameter-tuning method

**Generalized stochastic resonance theory.** As mentioned before, the noise intensity  $D$ , the system parameters  $a, b$  and the signal frequency  $f_0$  influence the outcomes of the nonlinear system directly [7-10]. The three groups of parameters correspond to the essential factors in SR respectively, which can be defined as the generalized parameters. Accordingly, the generalized SR methods have the uniform mechanism. The manner is to change one factor's feature by adjusting the related parameters in order to adapt to the other factors, and finally build new cooperation.

Not only the system parameters, but also the noise intensity exerts the influence on Kramers rate  $R_k$ . Reviewing the microcosmic explanation of SR, we can find that as SR occurs, the particle's average transition speed, which is half of Kramers rate, equals to the frequency of the periodic signal[11], i.e.,

$$f_0 = \frac{1}{2} R_k = \frac{a}{2\sqrt{2\pi}} e^{-a^2/4bD} . \quad (3)$$

Eq. 3 associates the noise intensity  $D$  and the system parameters with the driving frequency  $f_0$ . The three ways mentioned above take on the accordant physical meaning. Tuning the noise intensity or the system parameters is to make half of the Kramers rate tend to the large frequency of the real signal, while choosing the frequency scale ratio of twice sampling SR is to map or transform the actual signal frequency onto the SR frequency scale.

**United parameter-tuning SR.** The parameter-tuning SR method is helpful to treat the system with heavy noise, and the twice sampling method has an advantage on processing the input signal with the large frequency. Moreover, the actions of the bistable system parameters can build the system behavior in an orderly way, together with the twice sampling frequency. It is just the united parameter-tuning SR method.

Firstly, select the twice sampling frequency according to the estimative noise intensity in practice. By this way, the proper frequency scale ratio can transform the large frequency into the low frequency region, i.e., from  $f_0$  to  $f'_0$ . Secondly, adjust the system parameters. This step is to make the rational noise intensity required by the normalized frequency  $f'_0$ . The approach is shown in Fig. 1. Its application is presented as follows.

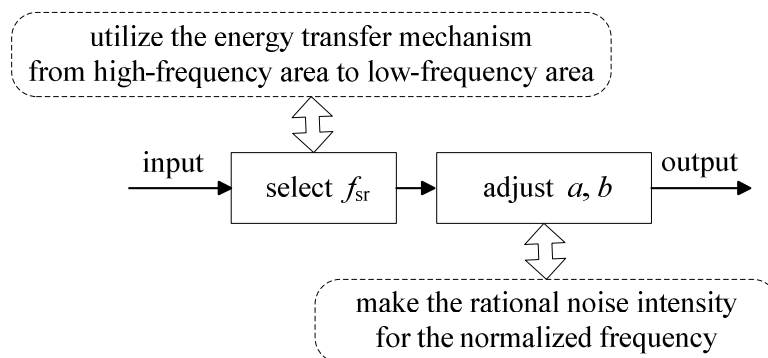


Fig.1 Process of the united parameter-tuning SR method

### Vibration test of flow meter system

**Engineering background and testing system.** The flow meter is a kind of equipment in process automation. Its precision is important to the manufacture. The engineering application was to solve the problem that the flow meter vibrated abnormally. The test aimed at determining the vibration sources to improve the structure. Fig.2 is the schematic diagram of the flow meter system. Fig.3 is the photograph of the test occasion.

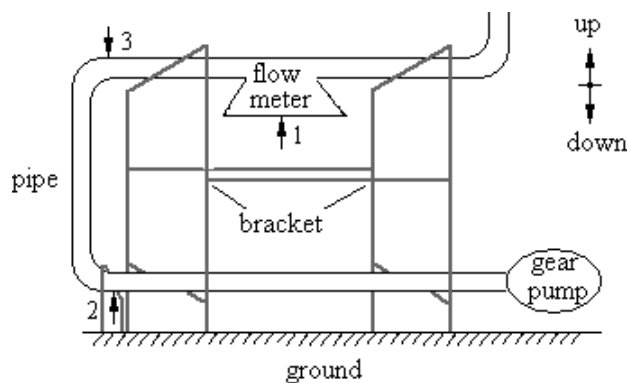


Fig.2 Frame of the flow meter system Fig.3 Photograph of the flow meter test occasion

The flow meter was composed of the gear pump, the pipes, the brackets and the flow meter. The acceleration transducers were laid at the measuring points, such as Point. 1 located at the flow meter. The vibration data collected by transducers were sent to the signal processing system. The test was carried out under different operating conditions. The following example was a part of it.

The actuator motor drove the gear pump. Its rated speed was 1400r/min, i.e., the working frequency was 24Hz. The rated speed of gear pump was 480r/min and the working frequency was 8Hz. The vibration frequency of flow meter was 105Hz.